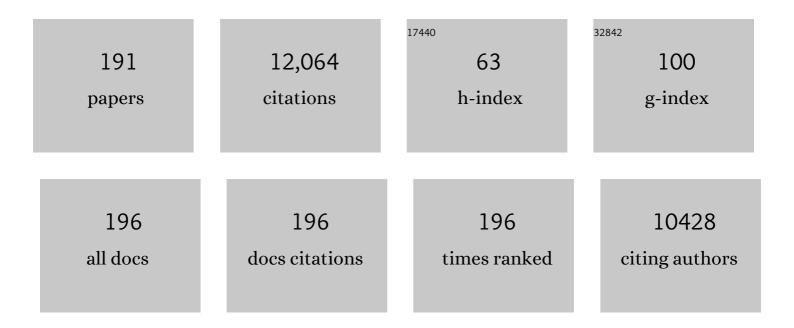
List of Publications by Year in descending order

Source: https://exaly.com/author-pdf/7272085/publications.pdf Version: 2024-02-01



Плинил Ни

#	Article	IF	CITATIONS
1	Constructing oxygen-deficient V2O3@C nanospheres for high performance potassium ion batteries. Chinese Chemical Letters, 2023, 34, 107372.	9.0	4
2	In-plane grain boundary induced defect state in hierarchical NiCo-LDH and effect on battery-type charge storage. Nano Research, 2023, 16, 4908-4916.	10.4	31
3	Enabling Argyrodite Sulfides as Superb Solidâ€State Electrolyte with Remarkable Interfacial Stability Against Electrodes. Energy and Environmental Materials, 2022, 5, 852-864.	12.8	43
4	Hierarchical nanocomposite of carbon-fiber-supported NiCo-based layered double-hydroxide nanosheets decorated with (NiCo)Se2 nanoparticles for high performance energy storage. Journal of Colloid and Interface Science, 2022, 608, 175-185.	9.4	41
5	3D frame-like architecture of N-C-incorporated mixed metal phosphide boosting ultrahigh energy density pouch-type supercapacitors. Nano Energy, 2022, 91, 106630.	16.0	74
6	Bimetallic atomic site catalysts for CO2 reduction reactions: a review. Environmental Chemistry Letters, 2022, 20, 243-262.	16.2	31
7	Mechanism of enhanced H2S sensor ability based on emerging Li0.5La0.5TiO3-SnO2 core-shell structure. Sensors and Actuators B: Chemical, 2022, 352, 131054.	7.8	13
8	Optimizing Hydrogen Binding on Ru Sites with RuCo Alloy Nanosheets for Efficient Alkaline Hydrogen Evolution. Angewandte Chemie, 2022, 134, .	2.0	24
9	White Light Afterglow in Carbon Dots Achieved via Synergy between the Roomâ€Temperature Phosphorescence and the Delayed Fluorescence. Small, 2022, 18, e2105415.	10.0	44
10	Optimizing Hydrogen Binding on Ru Sites with RuCo Alloy Nanosheets for Efficient Alkaline Hydrogen Evolution. Angewandte Chemie - International Edition, 2022, 61, e202113664.	13.8	102
11	Bright and Efficient Pure Red Perovskite Nanocrystals Lightâ€Emitting Devices via In Situ Modification. Advanced Functional Materials, 2022, 32, .	14.9	24
12	Near solution-level conductivity of polyvinyl alcohol based electrolyte and the application for fully compliant Al-air battery. Chemical Engineering Journal, 2022, 431, 134283.	12.7	23
13	Identification of the active site during CF ₄ hydrolytic decomposition over γ-Al ₂ O ₃ . Environmental Science: Nano, 2022, 9, 954-963.	4.3	6
14	Hydroxyl radical induced from hydrogen peroxide by cobalt manganese oxides for ciprofloxacin degradation. Chinese Chemical Letters, 2022, 33, 5208-5212.	9.0	17
15	Electric-field promoted C–C coupling over Cu nanoneedles for CO2 electroreduction to C2 products. Chinese Journal of Catalysis, 2022, 43, 519-525.	14.0	34
16	CO2 reduction reaction pathways on single-atom Co sites: Impacts of local coordination environment. Chinese Journal of Catalysis, 2022, 43, 832-838.	14.0	18
17	High-performance alkaline water splitting by Ni nanoparticle-decorated Mo-Ni microrods: Enhanced ion adsorption by the local electric field. Chemical Engineering Journal, 2022, 435, 134860.	12.7	20
18	Nickel polyphthalocyanine with electronic localization at the nickel site for enhanced CO2 reduction reaction. Applied Catalysis B: Environmental, 2022, 306, 121093.	20.2	53

#	Article	IF	CITATIONS
19	Efficient and Stable CF ₃ PEAI-Passivated CsPbI ₃ QDs toward Red LEDs. ACS Applied Materials & Interfaces, 2022, 14, 8235-8242.	8.0	20
20	Accelerating CO ₂ Electroreduction to Multicarbon Products via Synergistic Electric–Thermal Field on Copper Nanoneedles. Journal of the American Chemical Society, 2022, 144, 3039-3049.	13.7	147
21	Ligand Engineering in Nickel Phthalocyanine to Boost the Electrocatalytic Reduction of CO ₂ . Advanced Functional Materials, 2022, 32, .	14.9	80
22	Toward layered MoS ₂ anode for harvesting superior lithium storage. RSC Advances, 2022, 12, 9917-9922.	3.6	0
23	Vertical Cu Nanoneedle Arrays Enhance the Local Electric Field Promoting C ₂ Hydrocarbons in the CO ₂ Electroreduction. Nano Letters, 2022, 22, 1963-1970.	9.1	95
24	Highly Stable and Efficient Mn ²⁺ Doping Zero-Dimension Cs ₂ Zn _{<i>x</i>} Pb _{1–<i>x</i>} Cl ₄ Alloyed Nanorods toward White Electroluminescent Light-Emitting Diodes. Journal of Physical Chemistry Letters, 2022, 13, 2379-2387.	4.6	5
25	Microstructural and mechanical evolution of amorphous Zr-Si with irradiation induced atomic reconfiguration and free volume variation. Surfaces and Interfaces, 2022, 30, 101890.	3.0	2
26	Tandem catalysis on adjacent active motifs of copper grain boundary for efficient CO2 electroreduction toward C2 products. Journal of Energy Chemistry, 2022, 70, 219-223.	12.9	29
27	PDGF-BB-derived supramolecular hydrogel for promoting skin wound healing. Journal of Nanobiotechnology, 2022, 20, 201.	9.1	37
28	Enabling high energy lithium metal batteries via single-crystal Ni-rich cathode material co-doping strategy. Nature Communications, 2022, 13, 2319.	12.8	143
29	Heterostructured Ni3S4/Co9S8 Encapsulated in Nitrogen-Doped Carbon Nanocubes for Advanced Potassium Storage. Chemical Engineering Journal, 2022, 446, 136829.	12.7	8
30	Regulating local charges of atomically dispersed Mo+ sites by nitrogen coordination on cobalt nanosheets to trigger water dissociation for boosted hydrogen evolution in alkaline media. Journal of Energy Chemistry, 2022, 72, 125-132.	12.9	17
31	On the thermal stability and oxidation resistance of Zr/X(Cr, Ni, Si) multilayer structure. Surface and Coatings Technology, 2022, 440, 128500.	4.8	1
32	O-Doping Configurations Reduce the Adsorption Energy Barrier of K-lons to Improve the Electrochemical Performance of Biomass-Derived Carbon. Micromachines, 2022, 13, 806.	2.9	1
33	Narrowband Near-Infrared Photodetectors Based on Perovskite Waveguide Devices. Journal of Physical Chemistry Letters, 2022, 13, 6057-6063.	4.6	7
34	Electrochemically intercalated intermediate induced exfoliation of few-layer MoS2 from molybdenite for long-life sodium storage. Science China Materials, 2021, 64, 115-127.	6.3	22
35	Vertical SrNbO ₂ N Nanorod Arrays for Solarâ€Driven Photoelectrochemical Water Splitting. Solar Rrl, 2021, 5, 2000448.	5.8	10
36	Planar Li growth on Li21Si5 modified Li metal for the stabilization of anode. Journal of Materials Science and Technology, 2021, 76, 156-165.	10.7	6

#	Article	IF	CITATIONS
37	Self-consistent assessment of Li+ ion cathodes: Theory vs. experiments. Journal of Energy Chemistry, 2021, 59, 229-241.	12.9	22
38	Recent Advances in Strategies for Improving the Performance of CO ₂ Reduction Reaction on Single Atom Catalysts. Small Science, 2021, 1, 2000028.	9.9	57
39	Solution-Processed Efficient Perovskite Nanocrystal Light-Emitting Device Utilizing Doped Hole Transport Layer. Journal of Physical Chemistry Letters, 2021, 12, 94-100.	4.6	24
40	Mn2+ ions doped lead-free zero-dimensional K3SbCl6 perovskite nanocrystals towards white light emitting diodes. Chemical Engineering Journal, 2021, 413, 127415.	12.7	33
41	CoS ₂ needle arrays induced a local pseudo-acidic environment for alkaline hydrogen evolution. Nanoscale, 2021, 13, 13604-13609.	5.6	37
42	The progress of nanomaterials for carbon dioxide capture <i>via</i> the adsorption process. Environmental Science: Nano, 2021, 8, 890-912.	4.3	28
43	CoSe@N-Doped Carbon Nanotubes as a Potassium-Ion Battery Anode with High Initial Coulombic Efficiency and Superior Capacity Retention. ACS Nano, 2021, 15, 1121-1132.	14.6	98
44	Dual Evolution in Defect and Morphology of Singleâ€Atom Dispersed Carbon Based Oxygen Electrocatalyst. Advanced Functional Materials, 2021, 31, 2010472.	14.9	78
45	Paired Ru‒O‒Mo ensemble for efficient and stable alkaline hydrogen evolution reaction. Nano Energy, 2021, 82, 105767.	16.0	86
46	Tuning Charge Distribution of FeN ₄ via External N for Enhanced Oxygen Reduction Reaction. ACS Catalysis, 2021, 11, 6304-6315.	11.2	114
47	Zifâ€Derived Electrocatalysis: Dual Evolution in Defect and Morphology of Singleâ€Atom Dispersed Carbon Based Oxygen Electrocatalyst (Adv. Funct. Mater. 19/2021). Advanced Functional Materials, 2021, 31, 2170132.	14.9	1
48	Chemical Identification of Catalytically Active Sites on Oxygenâ€doped Carbon Nanosheet to Decipher the High Activity for Electroâ€synthesis Hydrogen Peroxide. Angewandte Chemie - International Edition, 2021, 60, 16607-16614.	13.8	150
49	Chemical Identification of Catalytically Active Sites on Oxygenâ€doped Carbon Nanosheet to Decipher the High Activity for Electroâ€synthesis Hydrogen Peroxide. Angewandte Chemie, 2021, 133, 16743-16750.	2.0	34
50	Activation of CO2 on graphitic carbon nitride supported single-atom cobalt sites. Chemical Engineering Journal, 2021, 415, 128982.	12.7	76
51	Metal–Organic Frameworksâ€Derived Nitrogenâ€Doped Porous Carbon Nanocubes with Embedded Co Nanoparticles as Efficient Sulfur Immobilizers for Room Temperature Sodium–Sulfur Batteries. Small Methods, 2021, 5, e2100455.	8.6	48
52	Intermediate enrichment effect of porous Cu catalyst for CO2 electroreduction to C2 fuels. Electrochimica Acta, 2021, 388, 138552.	5.2	22
53	Suppressing the interlayer-gliding of layered P3-type K0.5Mn0.7Co0.2Fe0.1O2 cathode materials on electrochemical potassium-ion storage. Applied Physics Reviews, 2021, 8, .	11.3	13
54	Single Cobalt Atoms Decorated Nâ€doped Carbon Polyhedron Enabled Dendriteâ€Free Sodium Metal Anode. Small Methods, 2021, 5, e2100833.	8.6	25

#	Article	IF	CITATIONS
55	Tuning the electron structure enables the NiZn alloy for CO2 electroreduction to formate. Journal of Energy Chemistry, 2021, 63, 625-632.	12.9	38
56	Atomically Dispersed sâ€Block Magnesium Sites for Electroreduction of CO ₂ to CO. Angewandte Chemie, 2021, 133, 25445-25449.	2.0	22
57	Atomically Dispersed sâ€Block Magnesium Sites for Electroreduction of CO ₂ to CO. Angewandte Chemie - International Edition, 2021, 60, 25241-25245.	13.8	104
58	Tuning the intermediate reaction barriers by a CuPd catalyst to improve the selectivity of CO2 electroreduction to C2 products. Chinese Journal of Catalysis, 2021, 42, 1500-1508.	14.0	56
59	"Mechanical–electrochemical―coupling structure and the application as a three-dimensional current collector for lithium metal anode. Applied Surface Science, 2021, 563, 150247.	6.1	10
60	Encapsulating Co9S8 nanocrystals into CNT-reinforced N-doped carbon nanofibers as a chainmail-like electrocatalyst for advanced Li-S batteries with high sulfur loading. Chemical Engineering Journal, 2021, 423, 130246.	12.7	45
61	Leadâ€Free Halide Perovskites for Light Emission: Recent Advances and Perspectives. Advanced Science, 2021, 8, 2003334.	11.2	155
62	Machine Learning in Screening High Performance Electrocatalysts for CO ₂ Reduction. Small Methods, 2021, 5, e2100987.	8.6	60
63	Optimizing the Performance of Perovskite Nanocrystal LEDs Utilizing Cobalt Doping on a ZnO Electron Transport Layer. Journal of Physical Chemistry Letters, 2021, 12, 10112-10119.	4.6	18
64	Post-treatment of CsPbI3 nanocrystals by p-iodo-D-Phenylalanine for efficient perovskite LEDs. Materials Today Physics, 2021, 21, 100555.	6.0	10
65	Pathogenesis of Children's Allergic Diseases: Refocusing the Role of the Gut Microbiota. Frontiers in Physiology, 2021, 12, 749544.	2.8	18
66	The Relationship among Physical Activity, Intestinal Flora, and Cardiovascular Disease. Cardiovascular Therapeutics, 2021, 2021, 1-10.	2.5	6
67	A New Co-Free Ni-Rich LiNi _{0.8} Fe _{0.1} Mn _{0.1} O ₂ Cathode for Low-Cost Li-Ion Batteries. ACS Applied Materials & Interfaces, 2021, 13, 57341-57349.	8.0	13
68	MOFs-derived porous Mo2C–C nano-octahedrons enable high-performance lithium–sulfur batteries. Energy Storage Materials, 2020, 25, 547-554.	18.0	118
69	Chemical diversity of iron species and structure evolution during the oxidation of C14 Laves phase Zr(Fe,Nb)2 in subcritical environment. Corrosion Science, 2020, 162, 108218.	6.6	21
70	Enhancing Li-S redox kinetics by fabrication of a three dimensional Co/CoP@nitrogen-doped carbon electrocatalyst. Chemical Engineering Journal, 2020, 380, 122595.	12.7	70
71	Recent advances in the utilization of copper sulfide compounds for electrochemical CO2 reduction. Nano Materials Science, 2020, 2, 235-247.	8.8	45
72	A honeycomb-like nitrogen-doped carbon as high-performance anode for potassium-ion batteries. Chemical Engineering Journal, 2020, 384, 123328.	12.7	72

#	Article	IF	CITATIONS
73	Metallic MoO ₂ â€Modified Graphitic Carbon Nitride Boosting Photocatalytic CO ₂ Reduction via Schottky Junction. Solar Rrl, 2020, 4, 1900416.	5.8	59
74	Single-atom transition metals supported on black phosphorene for electrochemical nitrogen reduction. Nanoscale, 2020, 12, 4903-4908.	5.6	107
75	Nano-porous hollow Li _{0.5} La _{0.5} TiO ₃ spheres and electronic structure modulation for ultra-fast H ₂ S detection. Journal of Materials Chemistry A, 2020, 8, 2376-2386.	10.3	32
76	Graphitic carbon nitride based single-atom photocatalysts. Frontiers of Physics, 2020, 15, 1.	5.0	72
77	In-situ constructing Na3V2(PO4)2F3/carbon nanocubes for fast ion diffusion with high-performance Na+-storage. Chemical Engineering Journal, 2020, 387, 123952.	12.7	53
78	In-situ MOFs-derived hollow Co9S8 polyhedron welding on the top of MnCo2S4 nanoneedles for high performance hybrid supercapacitors. Chemical Engineering Journal, 2020, 391, 123541.	12.7	63
79	Preparation and application of ZrB2-SiCw composite powder for corrosion resistance improvement in Al2O3–ZrO2–C slide plate materials. Ceramics International, 2020, 46, 9817-9825.	4.8	17
80	P3-type K0.5Mn0.72Ni0.15Co0.13O2 microspheres as cathode materials for high performance potassium-ion batteries. Chemical Engineering Journal, 2020, 392, 123735.	12.7	39
81	Tailoring the structure of supported δ-MnO2 nanosheets to raise pseudocapacitance by surface-modified carbon cloth. Journal of Power Sources, 2020, 449, 227507.	7.8	19
82	Na+-storage properties derived from a high pseudocapacitive behavior for nitrogen-doped porous carbon anode. Materials Letters, 2020, 261, 127064.	2.6	5
83	Fe ₂ P-decorated N,P Codoped Carbon Synthesized via Direct Biological Recycling for Endurable Sulfur Encapsulation. ACS Central Science, 2020, 6, 1827-1834.	11.3	27
84	Heterogeneous structured MoSe ₂ –MoO ₃ quantum dots with enhanced sodium/potassium storage. Journal of Materials Chemistry A, 2020, 8, 23395-23403.	10.3	48
85	Structural Insight into the Abnormal Capacity of a Co-Substituted Tunnel-Type Na _{0.44} MnO ₂ Cathode for Sodium-Ion Batteries. ACS Applied Materials & Interfaces, 2020, 12, 47548-47555.	8.0	18
86	Oxidation behavior and chemical evolution of architecturally arranged Zr/Si multilayer at high temperature. Surface and Coatings Technology, 2020, 399, 126205.	4.8	9
87	Design, synthesis, and application of metal sulfides for Li–S batteries: progress and prospects. Journal of Materials Chemistry A, 2020, 8, 17848-17882.	10.3	85
88	MOF-derived Co ₉ S ₈ polyhedrons on NiCo ₂ S ₄ nanowires for high-performance hybrid supercapacitors. Inorganic Chemistry Frontiers, 2020, 7, 4092-4100.	6.0	55
89	Iron phthalocyanine with coordination induced electronic localization to boost oxygen reduction reaction. Nature Communications, 2020, 11, 4173.	12.8	358
90	Large Interlayer Spacing of Few-Layered Cobalt–Tin-Based Sulfide Providing Superior Sodium Storage. ACS Applied Materials & Interfaces, 2020, 12, 41546-41556.	8.0	11

#	Article	IF	CITATIONS
91	Enhancing CO ₂ reduction by suppressing hydrogen evolution with polytetrafluoroethylene protected copper nanoneedles. Journal of Materials Chemistry A, 2020, 8, 15936-15941.	10.3	78
92	Evolution of "Spinodal decomposition―like structures during the oxidation of Zr(Fe,Nb)2 under subcritical environment. Scripta Materialia, 2020, 187, 107-112.	5.2	13
93	Two-pronged approach to regulate Li etching for a stable anode. Journal of Power Sources, 2020, 455, 227988.	7.8	14
94	Highly Efficient Broadband Solarâ€Blind UV Photodetector Based on Gd ₂ O ₃ :Eu ³⁺ –PMMA Composite Film. Advanced Materials Interfaces, 2020, 7, 2000570.	3.7	12
95	Construction of heterostructured NiFe ₂ O ₄ -C nanorods by transition metal recycling from simulated electroplating sludge leaching solution for high performance lithium ion batteries. Nanoscale, 2020, 12, 13398-13406.	5.6	17
96	Three-dimensional nitrogen–sulfur codoped layered porous carbon nanosheets with sulfur-regulated nitrogen content as a high-performance anode material for potassium-ion batteries. Dalton Transactions, 2020, 49, 5108-5120.	3.3	9
97	Cobalt single atoms supported on N-doped carbon as an active and resilient sulfur host for lithium–sulfur batteries. Energy Storage Materials, 2020, 28, 196-204.	18.0	117
98	Plasma-treatment induced H2O dissociation for the enhancement of photocatalytic CO2 reduction to CH4 over graphitic carbon nitride. Applied Surface Science, 2020, 508, 145173.	6.1	44
99	Carbon Nanosheets Encapsulated NiSb Nanoparticles as Advanced Anode Materials for Lithiumâ€lon Batteries. Energy and Environmental Materials, 2020, 3, 186-191.	12.8	32
100	Heterointerface Engineering of Hierarchical Bi ₂ S ₃ /MoS ₂ with Selfâ€Generated Rich Phase Boundaries for Superior Sodium Storage Performance. Advanced Functional Materials, 2020, 30, 1910732.	14.9	151
101	Dendrite-free lithium metal anode with lithiophilic interphase from hierarchical frameworks by tuned nucleation. Energy Storage Materials, 2020, 27, 124-132.	18.0	98
102	In situ atomic-scale engineering of the chemistry and structure of the grain boundaries region of Li3La2/3-TiO3. Scripta Materialia, 2020, 185, 134-139.	5.2	15
103	Fe _{1â^'x} S@S-doped carbon core–shell heterostructured hollow spheres as highly reversible anode materials for sodium ion batteries. Journal of Materials Chemistry A, 2019, 7, 20229-20238.	10.3	80
104	Surficial Structure Retention Mechanism for LiNi _{0.8} Co _{0.15} Al _{0.05} O ₂ in a Full Gradient Cathode. ACS Applied Materials & Interfaces, 2019, 11, 31991-31996.	8.0	28
105	A designer fast Li-ion conductor Li6.25PS5.25Cl0.75 and its contribution to the polyethylene oxide based electrolyte. Applied Surface Science, 2019, 493, 1326-1333.	6.1	24
106	Lithium Ion Conductivity in Double Antiperovskite Li _{6.5} OS _{1.5} I _{1.5} : Alloying and Boundary Effects. ACS Applied Energy Materials, 2019, 2, 6288-6294.	5.1	38
107	Quantum-Dot-Derived Catalysts for CO2 Reduction Reaction. Joule, 2019, 3, 1703-1718.	24.0	106
108	Hybrids of PtRu Nanoclusters and Black Phosphorus Nanosheets for Highly Efficient Alkaline Hydrogen Evolution Reaction. ACS Catalysis, 2019, 9, 10870-10875.	11.2	86

#	Article	IF	CITATIONS
109	Heterostructured Nanocubeâ€Shaped Binary Sulfide (SnCo)S ₂ Interlaced with Sâ€Doped Graphene as a Highâ€Performance Anode for Advanced Na ⁺ Batteries. Advanced Functional Materials, 2019, 29, 1807971.	14.9	154
110	Rational Design of TiO–TiO ₂ Heterostructure/Polypyrrole as a Multifunctional Sulfur Host for Advanced Lithium–Sulfur Batteries. ACS Applied Materials & Interfaces, 2019, 11, 5055-5063.	8.0	91
111	In Situ Fabrication of Carbon-Encapsulated Fe ₇ X ₈ (X = S, Se) for Enhanced Sodium Storage. ACS Applied Materials & Interfaces, 2019, 11, 19040-19047.	8.0	63
112	Synergistic effect of cation ordered structure and grain boundary engineering on long-term cycling of Li0.35La0.55TiO3-based solid batteries. Journal of the European Ceramic Society, 2019, 39, 3332-3337.	5.7	31
113	Recent advances in different-dimension electrocatalysts for carbon dioxide reduction. Journal of Colloid and Interface Science, 2019, 550, 17-47.	9.4	26
114	A mechanism assessment for the anti-corrosion of zirconia coating under the condition of subcritical water corrosion. Corrosion Science, 2019, 152, 54-59.	6.6	38
115	MOF-Derived FeS/C Nanosheets for High Performance Lithium Ion Batteries. Nanomaterials, 2019, 9, 492.	4.1	23
116	Fabrication of SnS ₂ /Mn ₂ SnS ₄ /Carbon Heterostructures for Sodium-Ion Batteries with High Initial Coulombic Efficiency and Cycling Stability. ACS Nano, 2019, 13, 3666-3676.	14.6	205
117	One-dimensional Z-scheme TiO _{2/WO_{3 composite nanofibres for enhanced photocatalytic activity of hydrogen production. International Journal of Nanomanufacturing, 2019, 15, 227.}}	0.3	2
118	Size effect on the electrochemical reaction path and performance of nano size phosphorus rich skutterudite nickle phosphide. Journal of Alloys and Compounds, 2019, 781, 1059-1068.	5.5	11
119	One-pot synthesis of SnS/C nanocomposites on carbon paper as a high-performance free-standing anode for lithium ion batteries. Journal of Alloys and Compounds, 2019, 779, 67-73.	5.5	19
120	N/S codoped carbon microboxes with expanded interlayer distance toward excellent potassium storage. Chemical Engineering Journal, 2019, 358, 1147-1154.	12.7	112
121	Three-dimensional (3D) flower-like MoSe2/N-doped carbon composite as a long-life and high-rate anode material for sodium-ion batteries. Chemical Engineering Journal, 2019, 357, 226-236.	12.7	92
122	A renewable natural cotton derived and nitrogen/sulfur co-doped carbon as a high-performance sodium ion battery anode. Materials Today Energy, 2018, 8, 37-44.	4.7	61
123	Constructing 2D layered MoS 2 nanosheets-modified Z-scheme TiO 2 /WO 3 nanofibers ternary nanojunction with enhanced photocatalytic activity. Applied Surface Science, 2018, 430, 466-474.	6.1	92
124	Dominant growth of higher manganese silicide film on Si substrate by introducing a Si oxide capping layer. Journal of Alloys and Compounds, 2018, 740, 541-544.	5.5	10
125	MoS ₂ -covered SnS nanosheets as anode material for lithium-ion batteries with high capacity and long cycle life. Journal of Materials Chemistry A, 2018, 6, 592-598.	10.3	142
126	Mn doped NaV3(PO4)3/C anode with high-rate and long cycle-life for sodium ion batteries. Energy Storage Materials, 2018, 12, 153-160.	18.0	55

#	Article	IF	CITATIONS
127	Strong interplay between dopant and SnO2 in amorphous transparent (Sn, Nb)O2 anode with high conductivity in electrochemical cycling. Journal of Alloys and Compounds, 2018, 735, 2401-2409.	5.5	28
128	Suppression on allotropic transformation of Sn planar anode with enhanced electrochemical performance. Applied Surface Science, 2018, 435, 1150-1158.	6.1	18
129	Chemically activated hollow carbon nanospheres as a high-performance anode material for potassium ion batteries. Journal of Materials Chemistry A, 2018, 6, 24317-24323.	10.3	174
130	Direct synthesis of FeS/N-doped carbon composite for high-performance sodium-ion batteries. Journal of Materials Chemistry A, 2018, 6, 24702-24708.	10.3	46
131	Construction of MoS ₂ /C Hierarchical Tubular Heterostructures for High-Performance Sodium Ion Batteries. ACS Nano, 2018, 12, 12578-12586.	14.6	272
132	Mechanistic Origin of the High Performance of Yolk@Shell Bi ₂ S ₃ @N-Doped Carbon Nanowire Electrodes. ACS Nano, 2018, 12, 12597-12611.	14.6	213
133	Activated Amorphous Carbon With High-Porosity Derived From Camellia Pollen Grains as Anode Materials for Lithium/Sodium Ion Batteries. Frontiers in Chemistry, 2018, 6, 366.	3.6	47
134	High pyridine N-doped porous carbon derived from metal–organic frameworks for boosting potassium-ion storage. Journal of Materials Chemistry A, 2018, 6, 17959-17966.	10.3	134
135	Nitrogen-doped bamboo-like carbon nanotubes as anode material for high performance potassium ion batteries. Journal of Materials Chemistry A, 2018, 6, 15162-15169.	10.3	161
136	RGO-functionalized polymer nanofibrous membrane with exceptional surface activity and ultra-low airflow resistance for PM _{2.5} filtration. Environmental Science: Nano, 2018, 5, 1813-1820.	4.3	47
137	A novel three-dimensional hierarchical NiCo2O4/Ni2P electrode for high energy asymmetric supercapacitor. Chemical Engineering Journal, 2018, 354, 254-260.	12.7	116
138	The formation and stacking faults of Fe and Cr containing Laves phase in Zircaloy-4 alloy. Materials Letters, 2017, 191, 203-205.	2.6	32
139	MoS 2 encapsulated SnO 2 -SnS/C nanosheets as a high performance anode material for lithium ion batteries. Chemical Engineering Journal, 2017, 316, 393-400.	12.7	136
140	In situ X-ray diffraction characterization of NiSe2 as a promising anode material for sodium ion batteries. Journal of Power Sources, 2017, 343, 483-491.	7.8	155
141	A New rGOâ€Overcoated Sb ₂ Se ₃ Nanorods Anode for Na ⁺ Battery: In Situ Xâ€Ray Diffraction Study on a Live Sodiation/Desodiation Process. Advanced Functional Materials, 2017, 27, 1606242.	14.9	258
142	Stabilizing the Nanostructure of SnO ₂ Anodes by Transition Metals: A Route to Achieve High Initial Coulombic Efficiency and Stable Capacities for Lithium Storage. Advanced Materials, 2017, 29, 1605006.	21.0	306
143	Snâ€MoS ₂ @C Microspheres as a Sodiumâ€Ion Battery Anode Material with High Capacity and Long Cycle Life. Chemistry - A European Journal, 2017, 23, 5051-5058.	3.3	39
144	MoS ₂ Decorated Fe ₃ O ₄ /Fe _{1–<i>x</i>} S@C Nanosheets as High-Performance Anode Materials for Lithium Ion and Sodium Ion Batteries. ACS Sustainable Chemistry and Engineering, 2017, 5, 4739-4745.	6.7	70

#	Article	IF	CITATIONS
145	V ₅ S ₈ –graphite hybrid nanosheets as a high rate-capacity and stable anode material for sodium-ion batteries. Energy and Environmental Science, 2017, 10, 107-113.	30.8	274
146	Plasmon enhancement on photocatalytic hydrogen production over the Z-scheme photosynthetic heterojunction system. Applied Catalysis B: Environmental, 2017, 210, 297-305.	20.2	107
147	Surface Modification of Na ₃ V ₂ (PO ₄) ₃ by Nitrogen and Sulfur Dual-Doped Carbon Layer with Advanced Sodium Storage Property. ACS Applied Materials & Interfaces, 2017, 9, 13151-13162.	8.0	103
148	Pinecone biomass-derived hard carbon anodes for high-performance sodium-ion batteries. RSC Advances, 2017, 7, 41504-41511.	3.6	117
149	SnS nanoparticles electrostatically anchored on three-dimensional N-doped graphene as an active and durable anode for sodium-ion batteries. Energy and Environmental Science, 2017, 10, 1757-1763.	30.8	431
150	<i>In situ</i> coupling of Ti ₂ O with rutile TiO ₂ as a core–shell structure and its photocatalysis performance. RSC Advances, 2017, 7, 54662-54667.	3.6	13
151	Exploration of VPO ₄ as a new anode material for sodium-ion batteries. Chemical Communications, 2017, 53, 12696-12699.	4.1	26
152	One-dimensional Z-scheme TiO 2 /WO 3 /Pt heterostructures for enhanced hydrogen generation. Applied Surface Science, 2017, 391, 211-217.	6.1	99
153	Direct evidence of multichannel-improved charge-carrier mechanism for enhanced photocatalytic H2 evolution. Scientific Reports, 2017, 7, 16116.	3.3	22
154	Remote plasma sputtering deposited Nb-doped TiO2 with remarkable transparent conductivity. Solar Energy Materials and Solar Cells, 2016, 149, 310-319.	6.2	40
155	Formation of nanocrystalline δ-ZrH x in Zircoloy-4: Orientation relationship and twinning. Journal of Alloys and Compounds, 2016, 658, 494-499.	5.5	23
156	In Situ Fabrication of Nano Porous NiO-Capped Ni3P film as Anode for Li-Ion Battery with Different Lithiation Path and Significantly Enhanced Electrochemical Performance. Electrochimica Acta, 2016, 220, 258-266.	5.2	64
157	On the oxidation behavior of (Zr,Nb)2Fe under simulated nuclear reactor conditions. Corrosion Science, 2016, 112, 718-723.	6.6	55
158	Formation and fine-structures of nano-precipitates in ZIRLO. Journal of Alloys and Compounds, 2016, 687, 451-457.	5.5	18
159	Construction of solid-state Z-scheme carbon-modified TiO2/WO3 nanofibers with enhanced photocatalytic hydrogen production. Journal of Power Sources, 2016, 328, 28-36.	7.8	114
160	In situ X-ray diffraction characterization of NbS2 nanosheets as the anode material for sodium ion batteries. Journal of Power Sources, 2016, 325, 410-416.	7.8	99
161	The effect of cobalt doping on the morphology and electrochemical performance of high-voltage spinel LiNi0.5Mn1.5O4 cathode material. Solid State Ionics, 2016, 292, 70-74.	2.7	31
162	Dramatically enhanced reversibility of Li ₂ 0 in SnO ₂ -based electrodes: the effect of nanostructure on high initial reversible capacity. Energy and Environmental Science, 2016, 9, 595-603.	30.8	300

#	Article	IF	CITATIONS
163	Template-oriented synthesis of monodispersed SnS2@SnO2 hetero-nanoflowers for Cr(VI) photoreduction. Applied Catalysis B: Environmental, 2016, 192, 17-25.	20.2	108
164	3D CuO Network Supported TiO ₂ Nanosheets with Applications for Energy Storage and Water Splitting. Science of Advanced Materials, 2016, 8, 1256-1262.	0.7	27
165	Synthesis and structural control of silicon and silicide nanowires/microrods using metal chloride sources. Japanese Journal of Applied Physics, 2015, 54, 07JD02.	1.5	4
166	Nanoscale Surface Modification of Lithiumâ€Rich Layeredâ€Oxide Composite Cathodes for Suppressing Voltage Fade. Angewandte Chemie - International Edition, 2015, 54, 13058-13062.	13.8	331
167	Lightâ€Induced Ion Rectification in Zigzag Nanochannels. Chemistry - an Asian Journal, 2015, 10, 2733-2737.	3.3	24
168	Three-dimensional Porous Networks of Ultra-long Electrospun SnO2 Nanotubes with High Photocatalytic Performance. Nano-Micro Letters, 2015, 7, 86-95.	27.0	35
169	Strong temperature-dependent crystallization, phase transition, optical and electrical characteristics of p-type CuAlO ₂ thin films. Physical Chemistry Chemical Physics, 2015, 17, 557-562.	2.8	18
170	Photoelectric conversion performances of Mn doped TiO2 under >420nm visible light irradiation. Journal of Saudi Chemical Society, 2015, 19, 595-601.	5.2	20
171	Surfactants assisted synthesis and electrochemical properties of nano-LiFePO 4 /C cathode materials for low temperature applications. Journal of Power Sources, 2015, 288, 337-344.	7.8	49
172	Facile assembly of partly graphene-enveloped sulfur composites in double-solvent for lithium–sulfur batteries. Electrochimica Acta, 2015, 178, 564-570.	5.2	25
173	In situ fabrication of CoFe alloy nanoparticles structured (Pr0.4Sr0.6)3(Fe0.85Nb0.15)2O7 ceramic anode for direct hydrocarbon solid oxide fuel cells. Nano Energy, 2015, 11, 704-710.	16.0	173
174	SnO2-core carbon-shell composite nanotubes with enhanced photocurrent and photocatalytic performance. Applied Catalysis B: Environmental, 2015, 166-167, 193-201.	20.2	15
175	Chemically anchoring of TiO2 coating on OH-terminated Mg3(PO3)2 surface and its influence on the in vitro degradation resistance of Mg–Zn–Ca alloy. Applied Surface Science, 2014, 308, 38-42.	6.1	45
176	Growth of MnSi1.7 Layers on MnSi Substrate by Molten Salt Method. Journal of Electronic Materials, 2014, 43, 1487-1491.	2.2	5
177	Fabrication of Predominantly Mn ⁴⁺ â€Doped TiO ₂ Nanoparticles under Equilibrium Conditions and Their Application as Visible‣ight Photocatalyts. Chemistry - an Asian Journal, 2014, 9, 1904-1912.	3.3	44
178	Reactive vapor deposition and electrochemical performance of nano-structured magnesium silicide on silicon and silicon carbide substrates. Materials Science in Semiconductor Processing, 2014, 27, 873-876.	4.0	11
179	Dye-sensitized solar cells based on TiO2 nanoparticles/nanobelts double-layered film with improved photovoltaic performance. Applied Surface Science, 2014, 319, 75-82.	6.1	78
180	Functionalization of Biomass Carbonaceous Aerogels: Selective Preparation of MnO ₂ @CA Composites for Supercapacitors. ACS Applied Materials & Interfaces, 2014, 6, 9689-9697.	8.0	125

#	Article	IF	CITATIONS
181	Syntheses and structural characterizations of CrSi2 nanostructures using Si substrates under CrCl2 vapor. Journal of Crystal Growth, 2013, 365, 11-18.	1.5	9
182	Corrosion protection of Mgâ€Znâ€Yâ€Nd alloy by flowerâ€like nanostructured <scp>TiO₂</scp> film for vascular stent application. Journal of Chemical Technology and Biotechnology, 2013, 88, 2062-2066.	3.2	6
183	Composite coating prepared by micro-arc oxidation followed by sol–gel process and in vitro degradation properties. Applied Surface Science, 2012, 258, 2939-2943.	6.1	38
184	Fabrication of chitosan/magnesium phosphate composite coating and the in vitro degradation properties of coated magnesium alloy. Materials Letters, 2012, 73, 59-61.	2.6	82
185	Preparation and in vitro degradation of the composite coating with high adhesion strength on biodegradable Mg–Zn–Ca alloy. Materials Characterization, 2011, 62, 1158-1165.	4.4	50
186	Corrosion behavior of TiO2 films on Mg–Zn alloy in simulated body fluid. Applied Surface Science, 2011, 257, 4464-4467.	6.1	21
187	In vitro degradation of AZ31 magnesium alloy coated with nano TiO2 film by sol–gel method. Applied Surface Science, 2011, 257, 8772-8777.	6.1	99
188	Preparation and electrical properties of Mn silicides by reaction of MnCl2 and Si powder. Physics Procedia, 2011, 11, 138-141.	1.2	6
189	OPTICAL AND ELECTRONIC PROPERTIES OF M2Si (M = Mg, Ca, Sr) GROWN BY REACTIVE DEPOSITION TECHNIQUE. International Journal of Modern Physics B, 2010, 24, 3693-3699.	2.0	14
190	Corrosion protection of AZ31 magnesium alloy by a TiO2 coating prepared by LPD method. Surface and Coatings Technology, 2009, 203, 2017-2020.	4.8	57
191	Growth condition dependence of structural and electrical properties of Mg2Si layers grown on silicon substrates. Vacuum, 2009, 83, 1494-1497.	3.5	25